

SCIENTIFIC REPORTS



OPEN

Safety and Optimization of Metabolic Labeling of Endothelial Progenitor Cells for Tracking

Sang-Soo Han¹, Hye-Eun Shim¹, Soon-Jung Park², Byoung-Chul Kim³, Dong-Eun Lee⁴, Hyung-Min Chung², Sung-Hwan Moon² & Sun-Woong Kang^{1,5}

Metabolic labeling is one of the most powerful methods to label the live cell for *in vitro* and *in vivo* tracking. However, the cellular mechanisms by modified glycosylation due to metabolic agents are not fully understood. Therefore, metabolic labeling has not yet been widely used in EPC tracking and labeling. In this study, cell functional properties such as proliferation, migration and permeability and gene expression patterns of metabolic labeling agent-treated hUCB-EPCs were analyzed to demonstrate cellular effects of metabolic labeling agents. As the results, 10 μM Ac4ManNAz treatment had no effects on cellular function or gene regulations, however, higher concentration of Ac4ManNAz (>20 μM) led to the inhibition of functional properties (proliferation rate, viability and rate of endocytosis) and down-regulation of genes related to cell adhesion, PI3K/AKT, FGF and EGFR signaling pathways. Interestingly, the new blood vessel formation and angiogenic potential of hUCB-EPCs were not affected by Ac4ManNAz concentration. Based on our results, we suggest 10 μM as the optimal concentration of Ac4ManNAz for *in vivo* hUCB-EPC labeling and tracking. Additionally, we expect that our approach can be used for understanding the efficacy and safety of stem cell-based therapy *in vivo*.

Human umbilical cord blood-derived endothelial progenitor cells (hUCB-EPCs) have a great potential therapeutic impact in clinical trials of acute nervous system disorders, myocardial infarction and stroke¹⁻³. hUCB-EPCs have been also used to investigate the repair of injured vessels and neovascularization or regeneration of ischemic tissues and have been used for therapeutic re-endothelialization of vein graft because of their ability to induce neovascularization under ischemic conditions⁴⁻⁶. Moreover, hUCB-EPC can be obtained without extensive surgical procedure⁷ and are immediately available, there are no risks to the donor and there is a low risk of transmitting infectious diseases⁸. For these reasons, currently, hUCB-EPCs are the preferred tool for animal- and patient-based studies than other forms of pluripotent hematopoietic stem cells and mesenchymal stem cells for transplantation⁹⁻¹¹. However, many unknown factors, including their regenerative property, the fate of transplanted hUCB-EPCs, *in vivo* migration to the site of injury and *in situ* differentiation have yet to be exploited in more efficient ways to treat various diseases¹²⁻¹⁴.

For understanding biological mechanisms and the therapeutic effects of inoculated cells *in vivo*, cell labeling and tracking are very useful processes¹⁵. Although direct labeling with specific dyes or indirect labeling with genetic cell modifications and reporter genes¹⁶ have been used to observe unknown factors of transplanted hUCB-EPCs. These labeling methods have several safety and technical issues, such as photobleaching, quenching, sensitivity to pH changes and multiple labeling steps¹⁷. Recently, various techniques, including fluorescence, bioluminescence, positron emission tomography (PET), single photon emission computed tomography (SPECT) and magnetic resonance imaging (MRI), have been developed and used for hUCB-EPC labeling and tracking¹⁸⁻²¹. Many studies have used MRI methods with iron oxide- and ¹⁹F-based probes²²⁻²⁵. Wang *et al.* and Willenbrock *et al.* reported that magnetically labeled hUCB-EPCs in a mouse model were detectable for more than 7 days post-transplantation and have many advantages such as a simple and low-cost labeling, an effective imaging window and good signal intensity^{26,27}. However, MRI labeling is limited by the persistence of the *in vivo* signal even

¹Predictive Model Research Center, Korea Institute of Toxicology, Daejeon, Korea. ²Department of Stem Cell Biology, School of Medicine, Konkuk University, Seoul, Korea. ³The Genomics Institute, Ulsan National Institute of Science and Technology, Ulsan, Korea. ⁴Advanced Radiation Technology Institute, Korea Atomic Energy Research Institute, Jeonbuk, Korea. ⁵Department of Human and Environmental Toxicology, University of Science and Technology, Daejeon, Korea. Sang-Soo Han and Hye-Eun Shim contributed equally. Correspondence and requests for materials should be addressed to S.-H.M. (email: sunghwanmoon@kku.ac.kr) or S.-W.K. (email: swkang@kitox.re.kr)

after death of the transplanted cells, such that the MRI signal does not correlate with the viability of transplanted cells²⁸.

Metabolic labeling is the preferred labeling technique for tracking live cells because it has many advantages such as low background, correlation of cell survival and simple steps for cell labeling^{29,30}. In addition, the reaction produces very few toxic and non-toxic byproducts and therefore, metabolic labeling has advantages that apply to *in vivo* studies. Till now, the metabolic labeling technique in stem cells has been mostly used for detecting glycoprotein markers of mesenchymal stem cell differentiation³¹, for identifying or isolating live colon cancer stem cells³² and for quantifying protein abundance in embryonic stem cells (ESCs)³³. However, the cellular mechanisms by which modified glycosylation due to metabolic agents are not completely understood³⁴. Recently, Lee *et al.* reported that the metabolic labeling technique can stably label stem cells, but this study only focused on efficient labeling of stem cells³⁵.

In this study, to validate the safety and optimize the metabolic labeling method, we analyze cell functional properties, such as proliferation, migration and permeability and gene expression patterns of metabolic labeling agents-treated hUCB-EPCs. First, we screened the azido sugars for more efficient labeling of hUCB-EPCs. And then, we observed changes in basic cellular events including cell growth, migration, permeability and mitochondrial function. We analyzed transcriptomic changes by RNA-seq, functional characterization of hUCB-EPCs by observation of tube formation and marker gene expression using flow cytometric analysis.

Results

Screening of metabolic labeling agent for efficient labeling of hUCB-EPCs. Metabolic labeling method was described as the introduction of subtle modifications into monosaccharide precursors, such as in the case of introducing an azido group from azide-functionalized monosaccharides (tetra-acetylated N-azidoacetylmannosamine (Ac4ManNAz), tetra-acetylated N-azidoacetylgalactosamine (Ac4GalNAz), or tetra-acetylated N-azidoacetylglucosamine (Ac4GlcNAz)) via post-translational modification (PTM)³⁶. Once the azido group was introduced into cellular glycans, the glycosylation position and type of three azide-functionalized monosaccharides differed based on each sugar type³⁷. In detail, the Ac4ManNAz was metabolically converted to azido sialic acid derivative, which is used for N-linked glycosylation of cell surface proteins³⁸, whereas Ac4GlcNAz and Ac4GalNAz were predominantly used for O-linked glycosylation as a substitute for O-GlcNAc and O-GalNAc, which are attached to serine and threonine side chain of numerous intracellular proteins³⁹. When using metabolic labeling reagents, the choice of reagents was found to be very important for efficiently labeling the target cells. Thus, we first screened the metabolic labeling reagents for efficient labeling hUCB-EPCs.

Isolated hUCB-EPCs were treated with 10, 20, or 50 μ M Ac4ManNAz, Ac4GlcNAz, or Ac4GalNAz, which can easily access the modified surface and intracellular proteins with the azido group via PTM. hUCB-EPCs treated with three azido sugars did not show changes or differences in cell morphology (Fig. 1A). To analyze the incorporation of azido groups, Western blot analysis was performed as described in materials and methods. Interestingly, Ac4ManNAz treatment resulted in a higher generation efficiency of the azido group than Ac4GalNAz and Ac4GlcNAz treatment (Fig. 1B). Azido groups were incorporated into cytosolic and membrane proteins on hUCB-EPCs treated with Ac4ManNAz and the rate of incorporation of labeled proteins gradually increased relative to Ac4ManNAz concentration. However, hUCB-EPCs treated with 50 μ M Ac4GalNAz or Ac4GlcNAz generated only the modified proteins and Ac4GlcNAz treatment labeled membrane proteins. In addition, the generation of azido groups was determined by biorthogonal copper-free click chemistry with dye-labeled dibenzyl cyclooctyne (DBCO-Cy5) (Fig. 1C). Ac4ManNAz treatment resulted in higher labeling efficiency than Ac4GalNAz and Ac4GlcNAz, which was similar to results from the Western blot analysis. Thus, we finally selected Ac4ManNAz for metabolic labeling of hUCB-EPCs.

Bio-physiological effects of Ac4ManNAz-treated hUCB-EPCs. When hUCB-EPCs were treated with Ac4ManNAz, an abiotic azido group was introduced to native proteins by PTM. Additionally, Ac4ManNAz, which is an analog of ManNAc, was used as a carbon source⁴⁰. Generally, the carbon source concentration can impair many cellular functions such as cell proliferation, viability and permeability^{41,42}. Additionally, glycosylation of native proteins regulates their functions and kinetics and changes in glycosylation can alter cellular functions such as host cell surface interactions and modulation of cell signaling and gene expression⁴³. Thus, Ac4ManNAz labeling of hUCB-EPCs still introduces the possibility of altering cellular physiology.

To validate the influence of Ac4ManNAz on hUCB-EPCs, we firstly performed cytotoxic tests using CCK-8 assay and cell morphology assessment. Morphological study suggests that treatment of Ac4ManNAz did not affect significantly on cell morphology (Fig. 2A). However, the growth rate gradually decreased in hUCB-EPCs treated with >20 μ M Ac4ManNAz (Fig. 2B) and cell viability data showed that treatment of >20 μ M Ac4ManNAz significantly decreased cell viability, approximately 6.2% and 12.3% ($*p < 0.05$) at the concentrations 20 μ M and 50 μ M of Ac4ManNAz as compared to control (Fig. 2C). We furthermore examined the effects of Ac4ManNAz using *in vitro* wound healing assay. The scratch wounds were almost the same size in each experimental group at 0h; after 18 h, the difference in the reduction in wound size was not statistically significant in any Ac4ManNAz (10, 20 and 50 μ M) treatment group (Fig. 3). In addition, we analyzed the permeability of hUCB-EPCs treated with Ac4ManNAz using liposome-mediated transfection of a pcDNA3-eGFP plasmid and Qdot 525 probe. The results of the permeability test using eGFP showed no significant differences between the treated and untreated conditions (Fig. 4A,C). However, results from the Qdot analysis revealed a gradual decrease in the rate of endocytosis of hUCB-EPCs treated with >20 μ M Ac4ManNAz (Fig. 4B,D). These results suggested that the membrane fusion was not changed; however, the rate of endocytosis was reduced in cells treated with >20 μ M Ac4ManNAz.

Additionally, we conducted the reactive oxygen species (ROS) generation assay and assessment of mitochondrial membrane potential ($\Delta\Psi_m$) to analyze the apoptosis induction by Ac4ManNAz treatments. The Fig. 5A suggests that hUCB-EPCs treated with 50 μ M Ac4ManNAz significantly increased ROS intensity as compared

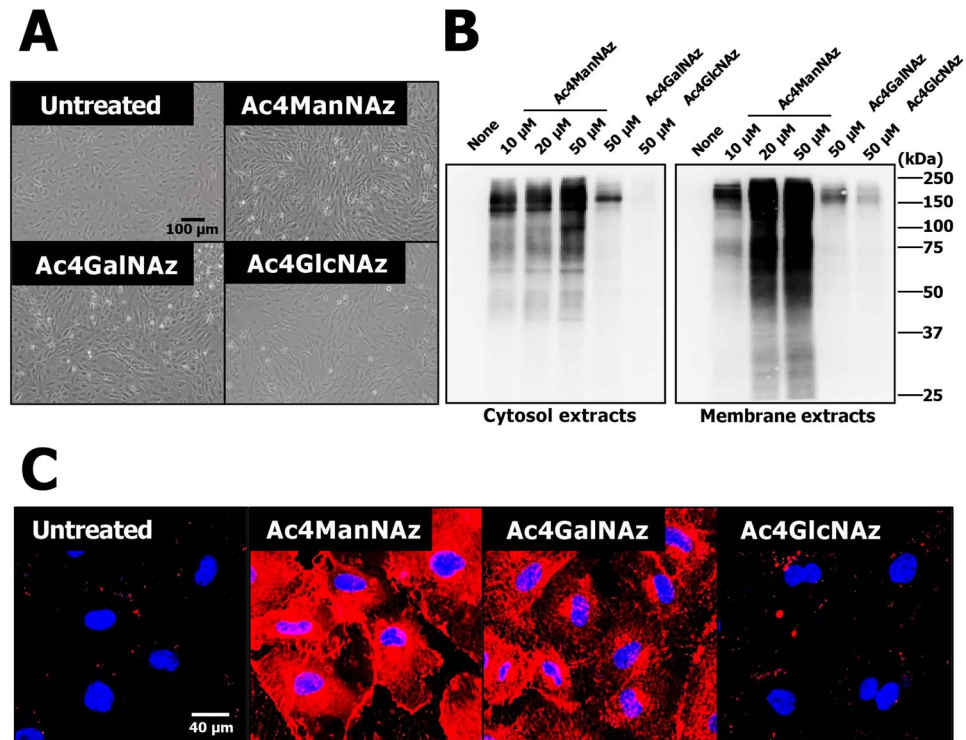


Figure 1. Screening metabolic labeling agents for hUCB-EPC labeling and tracking. (A) Morphological properties of hUCB-EPCs treated with three metabolic labeling agents (Ac4ManNAz, Ac4GlcNAz and Ac4GalNAz) were analyzed using microscopic observation. (B) Western blot analysis of metabolic labeling agent-treated hUCB-EPCs showing total proteins and generated azide groups. In the figure indicated full-length expression and all gels were run under the same experimental conditions while images of western blots displayed. (C) Visualization of metabolic labeling agent-treated hUCB-EPCs using DBCO-cy5 (n = 3).

to control. The quantitative measurement of ROS intensity was sustained increasingly to approximately 5.4% (* $p < 0.05$) at the concentrations 50 μM of Ac4ManNAz (Fig. 5C). The increased and decreased fluorescent intensity of red and green fluorescent caused by JC-1 indicates the change in mitochondrial membrane potential ($\Delta\Psi\text{m}$). Result indicated that hUCB-EPCs treated with 50 μM of Ac4ManNAz reduced a red fluorescence (Fig. 5B). As shown from quantitative data, the Green/Red-fluorescence cells ratio were increased to 1.5% at 50 μM of Ac4ManNAz treatment (Fig. 5D). Although increased ROS generation and reduced of JC-1 red fluorescence indicated potent apoptotic activity of treatment of 50 μM Ac4ManNAz, these changes are not clear which of them are directly associated with hUCB-EPCs apoptosis. To prove this, we additionally analyzed the apoptotic effects of Ac4ManNAz by Annexin V staining (Fig. S1). As the results, apoptosis rates of hUCB-EPCs treated with higher concentration (more than 20 μM) of Ac4ManNAz were not changed compared with non-treated hUCB-EPCs. These results described that high concentration of Ac4ManNAz slightly modulated the generation of ROS and mitochondrial membrane potential, but these changes were not induced apoptosis.

Transcriptomic change in Ac4ManNAz-treated hUCB-EPCs. To additionally address the metabolic labeling effects, we explored the transcriptome patterns of hUCB-EPCs treated with various concentrations of Ac4ManNAz. mRNA from hUCB-EPCs treated with 10, 20 and 50 μM of Ac4ManNAz and untreated hUCB-EPCs was extracted and analyzed using the HiSeq2000 platform. Next, based on the expression levels of known genes, we identified 615 genes that were changed by 2-fold or more with a threshold of “ $p < 0.05$ and $\text{FDR} < 5$ ”. And then, to identify cellular functional process-related genes, we carried out GO term analysis. Interestingly, in accordance with the increase in Ac4ManNAz concentration on hUCB-EPCs, 468 genes related to cell adhesion, cytokine-cytokine receptor interaction, extracellular matrix (ECM)-receptor interaction and cancer pathway were down-regulated (Fig. 6).

Of note, treatment with 20 and 50 μM Ac4ManNAz resulted in considerable down-regulation of many genes in the cell functional pathways of hUCB-EPCs. In cell adhesion, genes related to primary interactions with the cell matrix (LAMC3, ITGA5, ITGA10, ITGB8, TNR, EGFR and RELN) and integrin (CAMs) (ICAM1 and VCAM1), primary roles in cell-cell interactions (SELE), cell-cell interaction-mediated MHC (HLA-B, HLA-F and CD34) and collagen proteins (COL1A1, COL3A1, COL4A1, COL5A1 and COL6A2) were significantly down-regulated (Fig. 6A). In addition, genes related to cytokine-cytokine receptor interaction and ECM-receptor interaction were also down-regulated. In detail, gene expression levels of chemotactic cytokines (chemokines) (CCL2, CX3CL1, CXCL2, CXCL6, CXCL10, CXCL11 and CXCR4), tumor necrosis factors (TNFs) (TNFSF4, TNFSF10, TNFSF15, TNFSF18 and TNFRSF21), integrins (ITGA5, ITGA10, ITGB8) and ECM proteins (FN1, TNR and THBS1) were

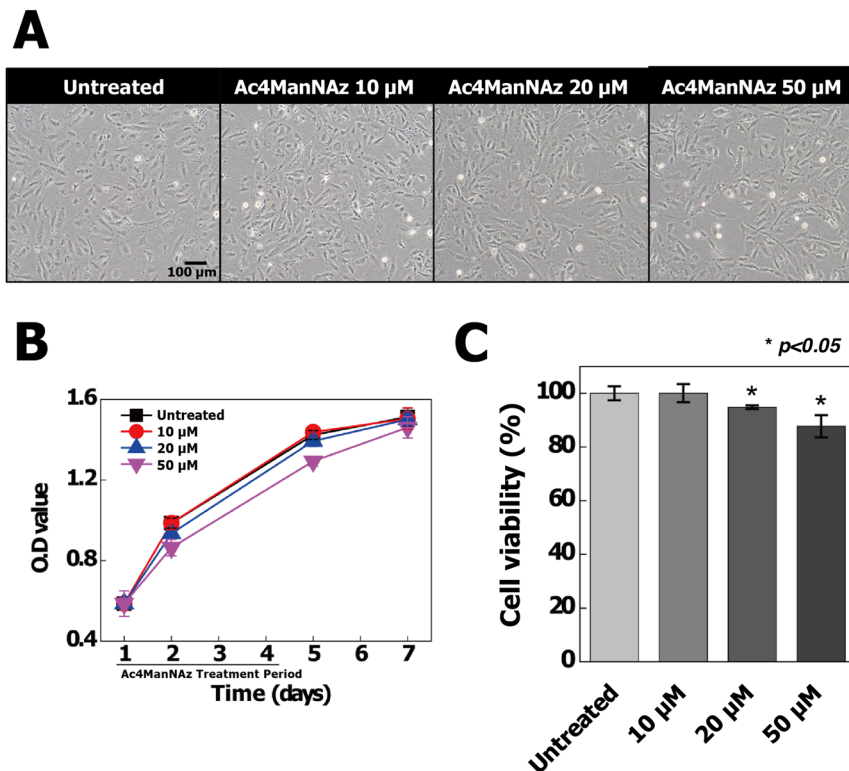


Figure 2. Analysis of morphological properties, proliferation ability and viability of Ac4ManNAz-treated hUCB-EPCs. All hUCB-EPCs were incubated with various concentrations of Ac4ManNAz (0 to 50 μ M). (A) Ac4ManNAz concentration-dependent morphological changes were analyzed by microscopic observation. Cell growth rate (B) and viability (C) were analyzed by CCK-8 and manual microscopic counting.

reduced by increasing the Ac4ManNAz concentration (Fig. 6B,C). Additionally, genes related to the regulation of cell cycle (CCNA1), cell growth, proliferation, apoptosis and the immune response (AKT3, STAT1, BIRC3, PTGS2, KIT, EGFR) were down-regulated (Fig. 6D). These results showed that Ac4ManNAz regulated a wide range of cell adhesion pathways and cell physiological pathways. In particular, these results also suggest that treatment >20 μ M Ac4ManNAz induces the immune response and inhibits cell cycle progression, cell proliferation and cell adhesion. Interestingly, contrary to previous reports, Ac4ManNAz modulated cell biological functions.

Analysis of hUCB-EPC functions after Ac4ManNAz treatment. In our results regarding the effects of metabolic labeling on hUCB-EPCs, higher concentrations of Ac4ManNAz negatively affected cell growth, proliferation, adhesion and rate of endocytosis and induction of ROS generation and mitochondrial depolarization. Of note, results from the gene expression analysis revealed the down-regulated expression of integrins, which are important for stem cell proliferation and self-renewal regulated via PI3K and focal adhesion kinase (FAK) signaling pathways⁴⁴. Additionally, AKT3 gene, which is downstream of the PI3K and FAK signaling pathways⁴⁵, was down-regulated. However, interestingly, there was no significant change in the gene expression of cadherin, which is one of the most important molecules in stem cell pluripotency and stemness^{46,47}. Stem cells are known to have two important characteristics that distinguish them from other types of cells⁴⁸. First, all stem cells are unspecialized. Second, under certain biochemical cues, stem cells can be induced to differentiate. Thus, as it was unclear whether Ac4ManNAz affects hUCB-EPC functions, we conducted the tubule formation assay and immunophenotyping of marker genes to analyze these important characteristics of EPCs.

To define the effects of Ac4ManNAz on hUCB-EPC functions, we carried out a tube formation assay on Matrigel to determine the angiogenic potential. We observed tube-like structures 4 days after treating hUCB-EPCs with 0, 10, 20 or 50 μ M Ac4ManNAz. The upper of Fig. 7A shows typical tube formation in all samples. One of the hallmarks of hUCB-EPCs is their ability to internalize ac-LDL via the “scavenger cell pathway” of LDL metabolism⁴⁹. At the endpoints of each protocol, we incubated our endothelial cultures with 1 μ g/mL ac-LDL conjugated with a fluorescent dye (Fig. 7A lower). In addition, the expression of specific endothelial cell surface markers CD31 (PECAM-1) and CD144 (VE-cadherin) of hUCB-EPCs were analyzed by flow cytometry (Fig. 7B). Interestingly, these results showed that Ac4ManNAz does not affect the natural characteristics of hUCB-EPCs.

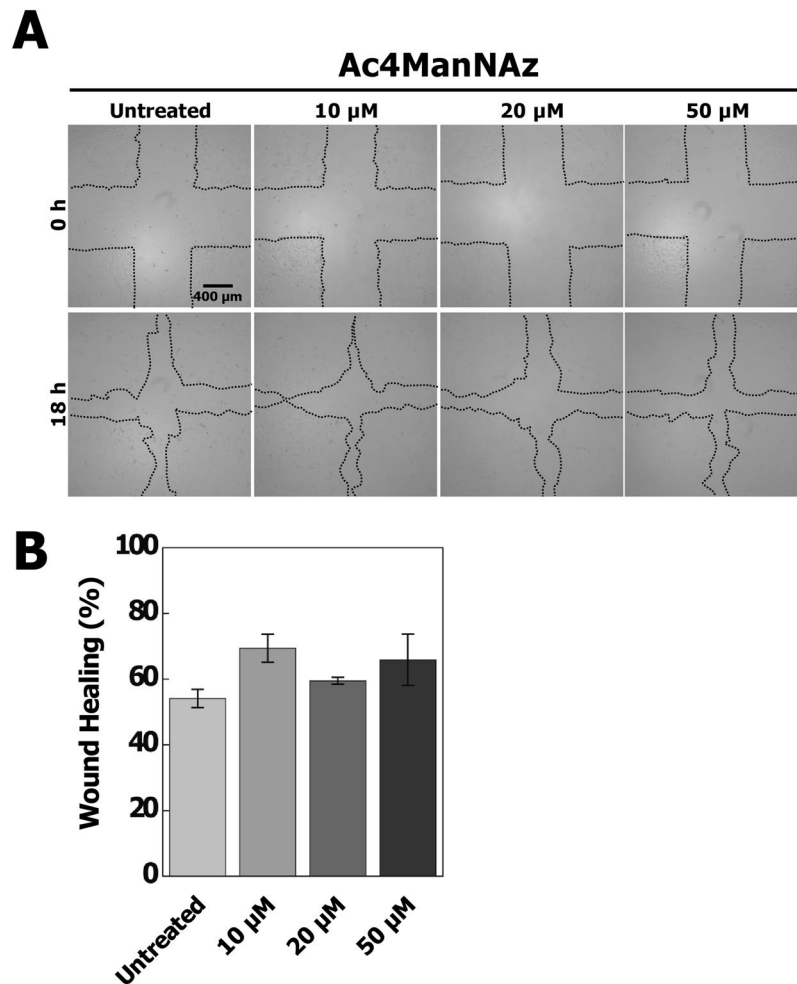


Figure 3. Wound healing assay in Ac4ManNAz-treated hUCB-EPCs. Wound healing assay was performed to assess the effect of Ac4ManNAz on the migration of hUCB-EPCs. The assay was repeated three times and representative images (A) and quantification (B) are shown.

Discussion

Stem cell-based therapy holds great promise for repairing damage and injury of the human body; however, the safety and efficacy of stem cell *in vivo* conditions have not been fully confirmed⁵⁰. Additionally, although hUCB-EPCs have great potential as therapeutics for cardiovascular diseases including coronary artery disease and stroke, the roles, behavior and fate of hUCB-EPCs *in vivo* are not completely understood⁵¹. Many cell labeling and tracking methods have been used and developed for hUCB-EPCs safety and efficacy *in vivo*¹⁷. Metabolic labeling is one of the most powerful methods for cell labeling and tracking and has proven to be superior to other imaging approaches^{29,30}. However, metabolic labeling has not yet been widely used in stem cell tracking, because the introduction of abiotic azido groups in native proteins via PTM can potentially affect cell signaling pathways, cell adhesion, cell proliferation and the immune response. We previously reported the effects of metabolic labeling agents on cancer cells, showing that a higher concentration of Ac4ManNAz, which was recommended to achieve the best labeling efficiency, led to inhibition of basic cellular properties and down-regulation of many genes related to cell biological functions⁵². Therefore, to successfully apply the metabolic labeling technique to EPC tracking and labeling, the effects of metabolic labeling agents must be demonstrated. Thus, in this study, we reported for the first time the effects and optimized conditions of a metabolic labeling agent in hUCB-EPCs.

Metabolic labeling agents are known to have three type of azido sugars (Ac4ManNAz, Ac4GalNAz and Ac4GlcNAz), which introduce the azido group onto a native protein using different glycosylation processes. Thus, we tested all azido sugars to screen for optimal metabolic labeling agents for hUCB-EPCs. As a result, treatments with Ac4GalNAz and Ac4GlcNAz showed weaker metabolic labeling efficiency than Ac4ManNAz. In addition, Ac4GlcNAz had very low labeling efficiency. Generally, O-glycosylated proteins are highly abundant in mammalian cells⁵³ and Ac4GalNAz and Ac4GlcNAz use the endogenous salvage pathway to introduce the azido group via O-linked glycosylation, which synthesizes UDP-GalNAc and GlcNAc from GalNAc and GlcNAc. Although these modification pathways involving numerous proteins, including various enzymes and nuclear pore proteins, are well-defined, conjugating an azido group on GalNAc and GlcNAc could be affected by enzyme function⁵⁴. Indeed, the Bertozzi research group has shown that AGX1 encodes UDP-GlcNAc pyrophosphorylase, which is

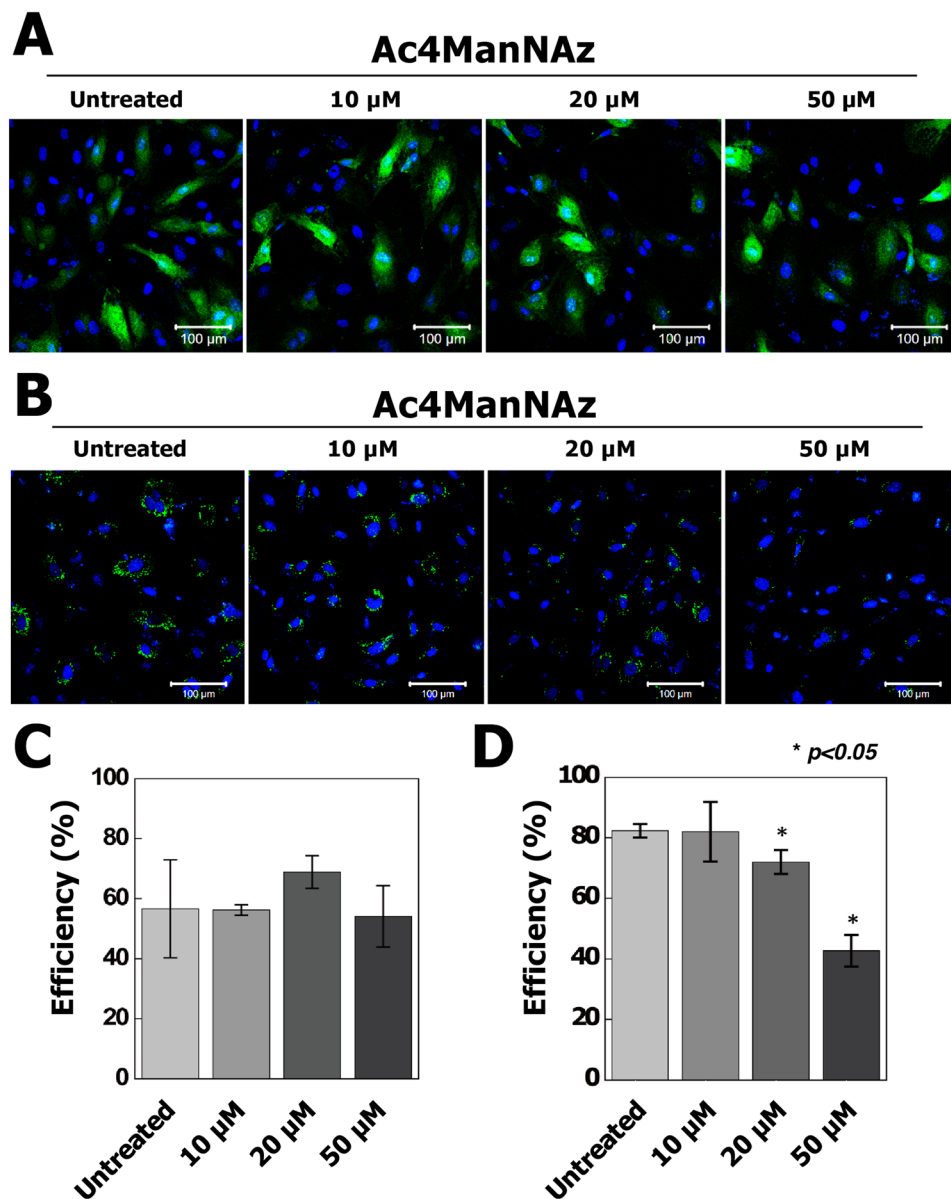


Figure 4. Analysis of cell permeability via transfection and Qdot 525 labeling in Ac4ManNAz-treated hUCB-EPCs. (A) Ac4ManNAz-treated hUCB-EPCs were transfected with pcDNA3-eGFP and GFP fluorescence and analyzed using fluorescence microscopy. (B) Confocal fluorescence images of live hUCB-EPC labeling with a Qdot 525 probe (green). Quantification of the transfection (C) and Qdot labeling (D) efficiency was conducted.

the final enzyme in UDP-GalNAc and GlcNAc biosynthesis and has the greatest loss of catalytic efficiency with azide-functionalized substrate analogs^{55,56}. However, our study was focused on the optimization of hUCB-EPC labeling using the metabolic labeling technique. Thus, we finally selected Ac4ManNAz.

In the manufacturer's procedure, the treatment of 50 μ M Ac4ManNAz as maximum level was recommended for the highest labeling efficiency. Also, many studies of cell or virus labeling and tracking was normally used in Ac4ManNAz concentration of 50 μ M or more^{57,58}. However, in our results, the decreased proliferation rate, viability, rate of endocytosis and induction of ROS generation and mitochondrial depolarization were caused by high concentration of Ac4ManNAz. The metabolic labeling agent Ac4ManNAz is composed of a sugar molecule (ManNAc) and an azido group, which are incorporated into cellular proteins. Therefore, Ac4ManNAz has the potential to affect metabolic flux and cellular mechanisms by addition of sugar molecules. Regarding this, in previous reports, a high concentration (1 mM) of ManNAc treatment in mouse ESCs induced switching of epigenetic factors from Sirt1/Ogt to Mgea5 at the Hcrt gene locus⁵⁹. A high concentration (>1,000 μ M) of Ac4ManNAc, which is a ManNAc analog without the azido group, dramatically increased cytotoxicity by inducing the accumulation of acetic acid in cells⁶⁰. Additionally, we previously analyzed the effects of ManNAc treatment on the A549 cancer cell line, ManNAc treatment at the same concentration of metabolic labeling agents does not affect cellular function or proliferation⁵². Also, the carbon energy source in the EGM-2-MV BulletKit Medium is the

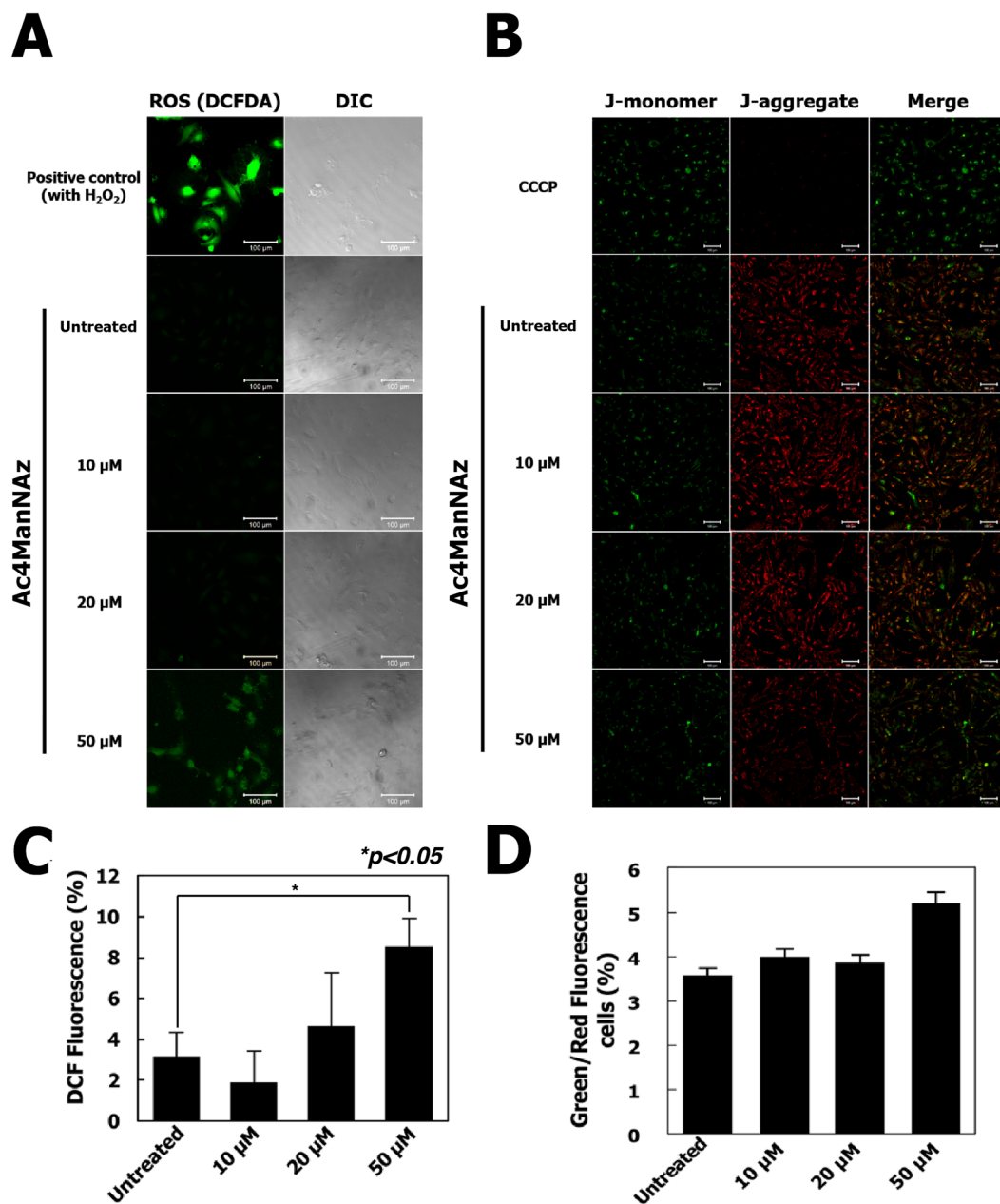


Figure 5. Analysis of reactive oxygen species (ROS) production and mitochondrial function in hUCB-EPCs treated with Ac4ManNAz. (A) hUCB-EPCs were treated with 0, 10, 20, or 50 μM Ac4ManNAz, and intracellular ROS levels were then measured using the fluorescent probe 2', 7'-dichlorofluorescein-diacetate (DCFH-DA). (B) Changes in mitochondrial membrane potential ($\Delta\Psi_m$) were measured in hUCB-EPCs using the fluorescent probe JC-1. (C) Quantification of ROS generation are expressed as the percentage of fluorescence intensity relative to the control. (D) Value of mitochondrial membrane potential were expressed as % Green/Red fluorescence cells.

5 mM. Ac4ManNAz were used less than 50 μM, which is a lower concentration by 100-fold. So, the addition of Ac4ManNAz as carbon energy source shown the negligible effects. These reports suggested that, changes of cellular physiology and mechanisms on hUCB-EPCs were caused by introduction of the azido group derived from Ac4ManNAz onto a native protein.

Non-toxic labeling method of azide group was the strain-promoted azide alkyne click chemistry (SPAAC) reaction, which rely on the use of cyclooctynes derivatives such as bicyclo[6.1.0]nonyne (BCN), difluorocyclooctyne (DIFO), dibenzylcyclooctyne (DIBO) and DBCO⁶¹. These cyclooctynes derivatives have high selectivity of azide-functionalized biomolecules. However, several groups have recently reported that thiol-reactive group (-SH) can be conjugated with various cyclooctyne derivatives in the presence of high thiol concentrations as thiol-yne reaction, which can lead to issues associated with nonspecific background labeling and affected the efficiency of biomolecules⁶²⁻⁶⁴. Nevertheless, in mammalian proteins, the occurrence frequency of cysteine

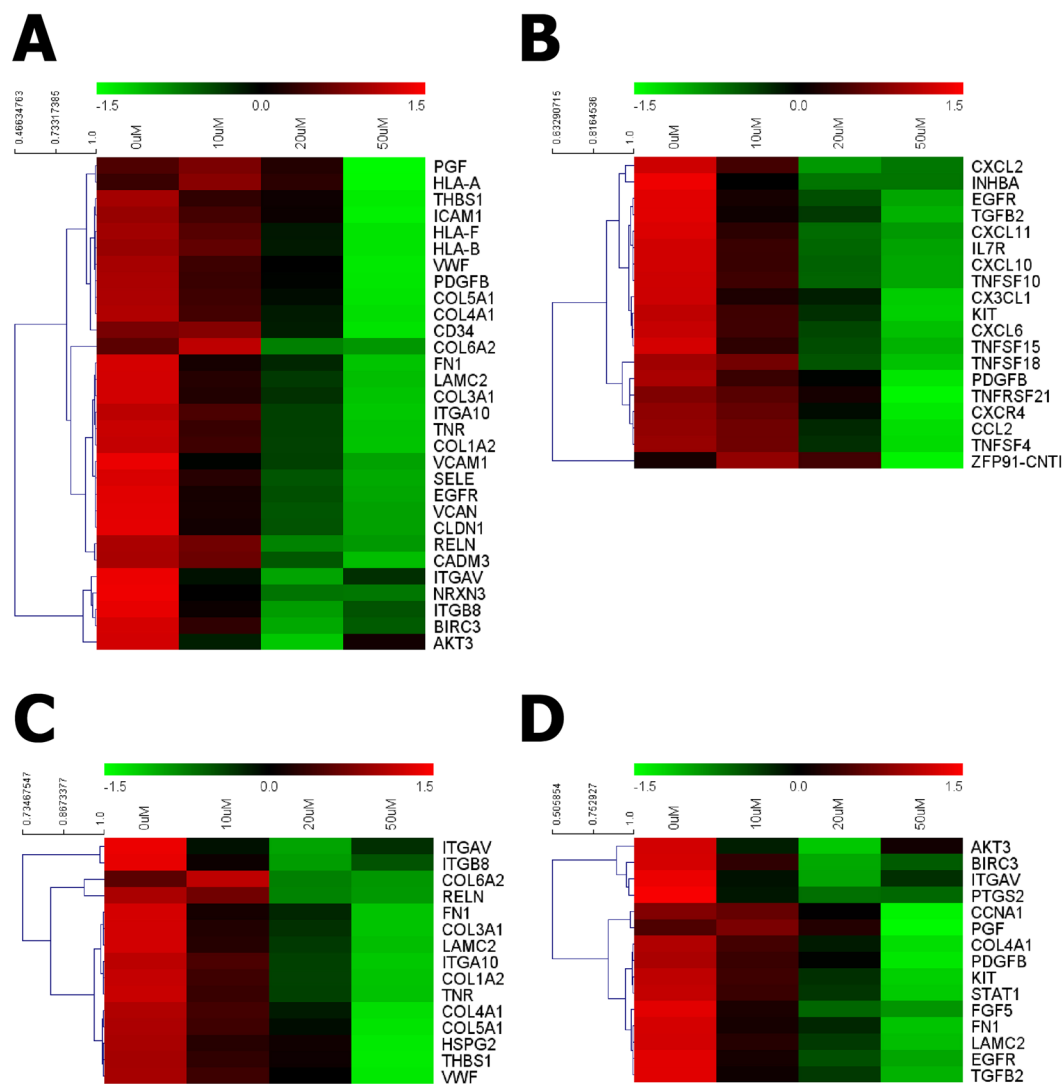


Figure 6. Transcriptomic analysis of effects of Ac4ManNAz treatment on hUCB-EPCs. Expression profiles of 0, 10, 20, and 50 μM Ac4ManNAz-treated hUCB-EPCs are shown. Heat map representation of mapped reads corresponds to protein-coding genes and the bio-functional pathway. (A) Cell adhesion, (B) cytokine-cytokine receptor interaction, (C) ECM-receptor interaction and (D) cancer-related pathways.

targets, which present the thiol group, is 3.3% and SPAAC reaction have the significantly higher reaction rates compared to thiol-yne reactions. For example, the BCN-azide reaction ($10^{-1} \text{ m}^{-1} \text{ s}^{-1}$) is approximately three orders of magnitude greater than the rate constant for the BCN-thiol reaction ($10^{-4} \text{ m}^{-1} \text{ s}^{-1}$)^{64–66}. In addition, Chin Fen Teo *et al.* optimized the ratio of the reaction between azido-DBCO functionalities to the formation of thiol-DBCO product. These results shown that the reaction to proceed longer than 1 hour leads to increase the non-specific thiol-DBCO reaction and azido-DBCO specific reaction reaches completion within 1 hour⁶⁷. Based on these results, in our experiments, hUCB-EPCs were treated with metabolic labeling agents supplemented medium (10, 20 and 50 μM) for 72 hours and all metabolic labeling agents-treated hUCB-EPCs were incubated with DBCO-Cy5 (10 μM , final concentration) for 1 hour at 37 °C. Thus, our optimized labeling procedures can be provided when highly specific labeling of hUCB-EPCs is required, thereby reducing the artifacts.

Our results reveal that the highly modified glycosylation by Ac4ManNAz treatments in hUCB-EPCs lead to a change in the physiological and biochemical properties of these cells. Notably, treatments with >20 μM Ac4ManNAz resulted in decreased growth rate, viability and rate of endocytosis and induction of ROS generation and mitochondrial depolarization. These results were consistent with a change in the expression of genes related to cell adhesion. Higher concentrations of Ac4ManNAz down-regulated the expression of integrin, collagen and fibronectin. Generally, integrins play an important role in various cell-signaling events including PI3K/AKT and FAK signaling pathways⁶⁸, which help to regulate stem cell proliferation and self-renewal⁶⁹. Accordingly, genes related to the PI3K/AKT, FGF and EGFR signaling pathways, which regulated cell proliferation, apoptosis, survival and immune response, were down-regulated^{46,70}. Interestingly, expression of cadherins, which are cell adhesion molecules that actively contribute to cell death, survival and proliferation, was not inhibited

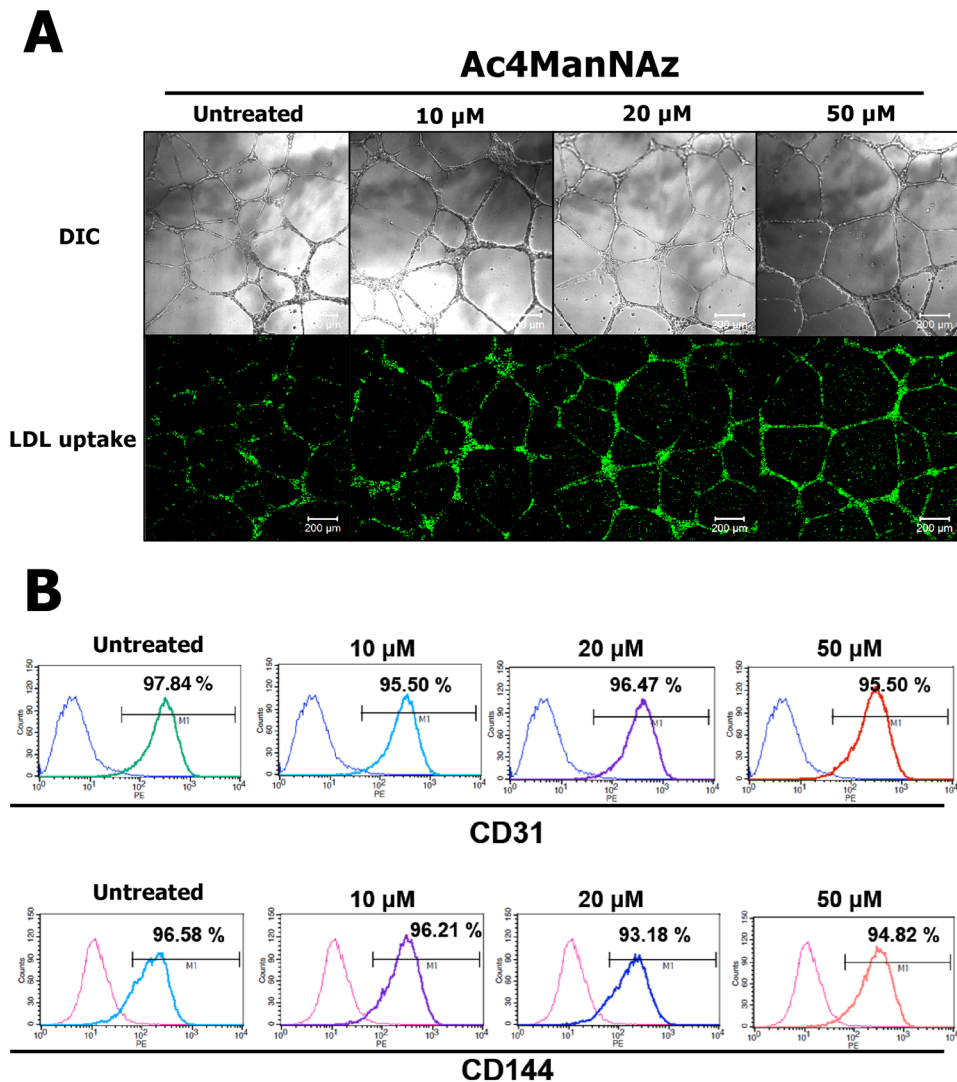


Figure 7. Analysis of tube formation and LDL uptake assay of Ac4ManNAz-treated hUCB-EPCs. (A) hUCB-EPCs treated with 0, 10, 20, or 50 μ M Ac4ManNAz were transferred to Matrigel-coated plates and cell rearrangement and tube structure formation were captured by a light microscope equipped with digital charge-coupled device camera after 48 h. Images of ac-LDL uptake were captured by fluorescence microscopy. (B) Representative FACS analysis demonstrated the function of hUCB-EPC by their markers CD31 and CD144.

by Ac4ManNAz treatments. The characterization of hUCB-EPCs were also not affected. Although treatments with $>20 \mu$ M Ac4ManNAz led to negative outcomes in hUCB-EPCs, the effects of treatments with control or 10 μ M Ac4ManNAz were not remarkably different. Additionally, it appears that 10 μ M Ac4ManNAz provides sufficient labeling for tracking and monitoring hUCB-EPCs (Fig. S2). Thus, we emphasize the treatment of 10 μ M Ac4ManNAz for labeling and tracking hUCB-EPCs as the optimal concentration because this concentration optimizes the proliferative capacity and functional property that are important for maximizing the use of EPCs as therapeutic agents.

In conclusion, this study described the optimal condition for the metabolic labeling technique for efficient labeling and tracking of hUCB-EPCs and the effects of metabolic labeling agents. Although high concentrations of Ac4ManNAz negatively affected hUCB-EPC properties, cell adhesion and cellular signaling pathways, 10 μ M Ac4ManNAz showed the least adverse effects when compared to untreated hUCB-EPCs and this concentration provided sufficient labeling efficiency for cell labeling and tracking. Based on our results, we suggest 10 μ M as the optimal concentration of Ac4ManNAz for *in vivo* cell labeling and tracking of hUCB-EPCs. Additionally, we expect that our approach can be used for understanding the efficacy and safety of stem cell-based therapy *in vivo* and to help determine the utility of stem cells in downstream experiments.

Methods

Ethic statement. All experiments were conducted in compliance with the relevant laws and institutional guidelines of the Korea Institute of Toxicology. The protocol was approved by the Committee on Biological Research of Korea Institute of Toxicology and Institutional Review Board (P01-201509-41-001).

hUCB-EPCs culture. hUCB-EPCs were purchased from AllCells (Alameda, CA, USA). hUCB-EPCs culture were performed as previously described^{71,72}. Briefly, mononuclear cells (MNCs) were first isolated from fresh hUCB-EPCs by density gradient centrifugation using Ficoll reagent (GE Healthcare, Piscataway, NJ, USA). MNCs were plated on fibronectin-coated tissue culture plates at a density of $3 \sim 6 \times 10^6$ cells/6 wells in EGM-2-MV BulletKit Medium (Lonza, Walkersville, MD, USA) and cells were maintained for 5–7 days and used as an enriched EPC population.

In vitro cell labeling and imaging. hUCB-EPCs (5×10^4 cells/35 mm glass-bottom dishes) were treated with Ac4ManNAz, Ac4GalNAz, or Ac4GlcNAz (Invitrogen, Carlsbad, CA, USA) supplemented medium (50 μ M, final concentration of each) for 72 h. Cells were washed twice with Dulbecco's phosphate-buffered saline (DPBS) and subsequently incubated with DBCO-Cy5 (10 μ M, final concentration) for 1 h at 37 °C. Cells were then washed and fixed with 4% paraformaldehyde for 15 min. After fixation, nuclei were stained with DAPI solution (Invitrogen, Carlsbad, CA, USA). All cell images were obtained using a confocal laser scanning microscope (Leica Microsystems, Mannheim, Germany) equipped with a 405 diode (405 nm) and HeNe-Red (633 nm) lasers.

Western blot analysis. To confirm the introduction of azide ($-N^3$) in the hUCB-EPCs, each 10–50 μ M of Ac4ManNAz-, Ac4GalNAz-, or Ac4GlcNAz-treated hUCB-EPCs (2×10^6 cells/100 mm dish) were prepared. Cells were washed twice with DPBS, pH 7.4 and harvested to extract cellular protein. A subcellular protein fractionation kit (Thermo Fisher Scientific, Rockford, IL, USA) was used according to the manufacturer's instructions for segregating proteins from different cellular compartments including cytosol, membrane, nucleus, chromatin and cytoskeletons. Protein lysate concentrations were individually determined by bicinchoninic acid (BCA) protein assay (Thermo Fisher Scientific, Rockford, IL, USA) and protein concentrations were adjusted to 1 mg/mL. Then, 100 μ L of lysate was incubated with 5 mM phosphine-PEG3-biotin in DPBS for 6 h at 37 °C to assess specific interactions between phosphine and an azide group of the cellular protein. Samples were boiled with SDS loading buffer and resolved by 10% SPS-PAGE and proteins were transferred to Hybond-P membrane (Amersham, St. Albans, UK). After blocking with 5% bovine serum albumin in TBST (50 mM Tris-HCl, 150 mM NaCl, 0.1% Tween-20, pH 7.4), the membrane was incubated in streptavidin-HRP (diluted 1:10,000 in TBST) overnight at 4 °C. Then, the membrane was washed three times with TBST and developed using ECL Western Blotting Substrate (Thermo Fisher Scientific, Rockford, IL, USA).

Cell viability and wound healing assay. To measure cell viability, hUCB-EPCs were seeded in 96-well plates (5×10^3 cells/well) and incubated for 1 day. Cells were incubated with various concentrations of Ac4ManNAz (0 to 50 μ M) for 3 days at 37 °C. Cell Counting Kit-8 solution (10 μ L) (Dojindo Molecular Technologies Inc., Kumamoto, Japan) was then added to each well. After further incubation for 2 h at 37 °C, the absorbance of each well was measured at 450 nm using a microplate reader (VersaMax™, Molecular Devices Corp., Sunnyvale, CA, USA). For wound healing, a sterile pipette tip was used to clear a small area across the diameter of 10 cm dishes with confluent monolayers of untreated or Ac4ManNAz-treated hUCB-EPCs. Cell migration was measured and photographed from the wound/scratch edge after 18 h.

Analysis of reactive oxygen species (ROS) generation and mitochondrial membrane potential. Microscopic fluorescence imaging was used to study reactive oxygen species (ROS) generation in hUCB-EPCs after treatments to different concentrations of Ac4ManNAz. Cells (1×10^4 per well) were seeded and were then treated to 0 μ M, 10 μ M, 20 μ M and 50 μ M concentrations of Ac4ManNAz for 3 days at 37 °C. Cells were incubated with 2,7-Dichlorodihydrofluorescein diacetate (DCF-DA) (10 mM) for 30 min at 37 °C. The reaction mixture was aspirated and replaced by 200 μ L of phosphate-buffered saline (PBS) in each well. The plate was kept on a shaker for 10 min at room temperature in the dark. An inverted fluorescent microscope was used to visualize intracellular fluorescence of cells and to capture images. Mitochondrial membrane potential was measured using JC-1 dye (5',6,6'-tetrachloro-1,1',3,3'-tetraethylbenzimidazolyl-carbocyanine iodide; Life Technologies, Eugene, Oregon, USA) according to the manufacturer's instructions. Briefly, hUCB-EPCs were grown in 24-well plate and treated with different concentrations of Ac4ManNAz. Ac4ManNAz-treated or untreated hUCB-EPCs were washed with PBS and stained with 10 μ g/mL JC-1 dye for 15 min at 37 °C and fluorescence images were acquired.

Transfection and Qdot 525 labeling. hUCB-EPCs were transfected with 100 ng of pcDNA3-EGFP using Lipofectamine 2000 (Invitrogen, Carlsbad, CA, USA) according to the manufacturer's instructions. In addition, 1 μ M Qdot 525 (Thermo Fisher Scientific, Rockford, IL, USA) in medium was incubated for 4–6 h at 37 °C and hUCB-EPC samples were diluted in DPBS immediately before measurement. Then, we analyzed samples using fluorescence microscopy.

RNA-seq analysis. hUCB-EPCs were cultured with 0, 10 or 50 μ M Ac4ManNAz and harvested. Total RNA was extracted with TRIzol reagent (Invitrogen, Carlsbad, CA, USA) and the quantity and quality of total RNA were evaluated using a NanoDrop spectrophotometer (NanoDrop Technologies, Montchanin, DE, USA) and a 2100 Bioanalyzer (Agilent Technologies, Palo Alto, CA, USA). An RNA sequencing library was generated using TruSeq RNA Library Preparation Kit (Illumina, San Diego, CA, USA) according to the user's instruction manual. Briefly, mRNA was separated from total RNA using Oligo (dT) beads and chemically fragmented. After double-strand cDNA synthesis of the fragmented mRNA, end-repair, adenylation of the 3'-end and sequencing adapter ligation were performed and followed by DNA purification with magnetic beads and PCR amplification. Finally, the amplified library was purified, quantified and then applied for template preparation. A HiSeq2000 platform was used to generate 99-bp paired-end sequencing reads (Illumina, San Diego, CA, USA). All 99-bp paired-end sequence reads were mapped to the human genome using TopHat version 2.0.4. Finally, we identified differentially expressed genes (DEgenes). To characterize the biological pathways related to differentially

expressed sequences and transcription factors, representative pathways were analyzed in the context of several databases such as KEGG (<http://www.genome.ad.jp>), BioCarta (<http://www.biocarta.com>) and Reactome (<http://www.reactome.org>), as suggested by MsigDB v4.0. Additionally, we used Fisher's exact test and FDR to examine mapping pathways (filtering options: $p < 0.05$ and $FDR < 5$). To identify cellular functional process-related genes, the DEgenes were subjected to gene ontology (GO) analysis using the Database for Annotation, Visualization and Integrated Discovery (DAVID), KEGG, BIOCARTE, REACTOME and Pathway Interaction Database (PID). We used a Gene Set Enrichment Analysis technique to identify statistically up- and down-regulated gene set.

In vitro tube formation assay. Functional characterization of hUCB-EPCs was performed using vascular tube formation and acetylated low-density lipoprotein (ac-LDL; Invitrogen, Carlsbad, CA, USA) uptake assays. For the vascular tube formation assay, 50 μ L of Matrigel Basement Membrane Matrix (BD Biosciences, San Diego, CA, USA) was added to a 48-well plate and allowed to solidify at 37 °C for 30 min; 5×10^4 hUCB-EPCs were suspended in 100 μ L of culture medium and plated onto the Matrigel layer. After 24 h, the medium was removed and the formation of vascular tube-like structures was assessed with an inverted microscope (Eclipse TS100; Nikon, Tokyo, Japan) and a digital camera system for imaging (Digital SLR Camera D300; Nikon, Tokyo, Japan). For the ac-LDL uptake assay, hUCB-EPCs were seeded onto glass coverslips in 24-well plates at a density of 5×10^4 cells/well in MV2 medium. When cells reached $\sim 80\%$ confluence, cultures were serum-deprived overnight in Iscove's Modified Dulbecco's Medium (IMDM, Sigma-Aldrich, St. Louis, MO, USA) supplemented with 2% lipoprotein-deficient serum from human plasma (Sigma-Aldrich, St. Louis, MO, USA) and then, the medium was replaced with IMDM supplemented with 100 μ g/mL human ac-LDL. After 24 h, cells on coverslips were stained with Nile Red (Sigma-Aldrich, St. Louis, MO, USA) and examined by fluorescence microscopy with an inverted microscope (Eclipse TS100; Nikon, Tokyo, Japan) and a digital camera system for imaging (Digital SLR Camera D300; Nikon, Tokyo, Japan).

Flow Cytometry. To analyze hUCB-EPC marker genes, immunophenotyping was performed using the following monoclonal antibodies: anti-CD31-FITC (1:25, BD Biosciences, San Jose, CA, USA) and anti-CD144-PE (1:10, Beckman Coulter, Fullerton, CA, USA). Antibodies and matched isotype control (Beckman Coulter, Fullerton, CA, USA) were incubated for 30 min at 4 °C. Data were acquired and analyzed on a five-parameter flow cytometer (FACSCalibur, Becton Dickinson, San Jose, CA) with Weasel software (WEHI, Melbourne, Australia).

Statistical analysis. Experimental data are presented as a mean \pm standard deviation and were analyzed using Analysis of Variance (ANOVA) tests. A value of $p < 0.05$ was considered statistically significant.

References

- Asahara, T. *et al.* Isolation of putative progenitor endothelial cells for angiogenesis. *Science* **275**, 964–967, <https://doi.org/10.1126/science.275.5302.964> (1997).
- Sukmawati, D. & Tanaka, R. Introduction to next generation of endothelial progenitor cell therapy: a promise in vascular medicine. *Am J Transl Res* **7**, 411–421 (2015).
- Zhao, Y. H. *et al.* Endothelial Progenitor Cells: Therapeutic Perspective for Ischemic Stroke. *Cns Neurosci Ther* **19**, 67–75, <https://doi.org/10.1111/cns.12040> (2013).
- Mitchell, K. E. *et al.* Matrix cells from Wharton's jelly form neurons and glia. *Stem Cells* **21**, 50–60 (2003).
- Schmidt, D. *et al.* Umbilical cord blood derived endothelial progenitor cells for tissue engineering of vascular grafts. *Ann Thorac Surg* **78**, 2094–2098, <https://doi.org/10.1016/j.athoracsur.2004.06.052> (2004).
- Yang, H. M. *et al.* Therapeutic Efficacy of Human Embryonic Stem Cell-Derived Endothelial Cells in Humanized Mouse Models Harboring a Human Immune System. *Arterioscl Throm Vas* **33**, 2839–2849, <https://doi.org/10.1161/Atvbaha.113.302462> (2013).
- Ingram, D. A. *et al.* Identification of a novel hierarchy of endothelial progenitor cells using human peripheral and umbilical cord blood. *Blood* **104**, 2752–2760, <https://doi.org/10.1182/blood-2004-04-1396> (2004).
- Rocha, V. & Gluckman, E. Improving outcomes of cord blood transplantation: HLA matching, cell dose and other graft- and transplantation-related factors. *British journal of haematology* **147**, 262–274, <https://doi.org/10.1111/j.1365-2141.2009.07883.x> (2009).
- Madhambayan, G. & Rogers, I. Umbilical cord-derived stem cells for tissue therapy: current and future uses. *Regenerative medicine* **1**, 777–787, <https://doi.org/10.2217/17460751.1.6.777> (2006).
- Bliss, T., Guzman, R., Daadi, M. & Steinberg, G. K. Cell transplantation therapy for stroke. *Stroke* **38**, 817–826, <https://doi.org/10.1161/01.Str.0000247888.25985.62> (2007).
- Laughlin, M. J. *et al.* Outcomes after transplantation of cord blood or bone marrow from unrelated donors in adults with leukemia. *New Engl J Med* **351**, 2265–2275, <https://doi.org/10.1056/NEJMoa041276> (2004).
- Li, Y.-F. *et al.* Endothelial progenitor cells in ischemic stroke: an exploration from hypothesis to therapy. *Journal of Hematology & Oncology* **8**, 33, <https://doi.org/10.1186/s13045-015-0130-8> (2015).
- Song, E., Lu, C.-W., Fang, L.-J. & Yang, W. Culture and identification of endothelial progenitor cells from human umbilical cord blood. *International Journal of Ophthalmology* **3**, 49–53, <https://doi.org/10.3980/j.issn.2222-3959.2010.01.11> (2010).
- Sudchada, S. *et al.* CD14⁺/CD34⁺ is the founding population of umbilical cord blood-derived endothelial progenitor cells and angiogenin1 is an important factor promoting the colony formation. *Annals of Hematology* **91**, 321–329, <https://doi.org/10.1007/s00277-011-1303-3> (2012).
- Wang, J. & Jokerst, J. V. Stem Cell Imaging: Tools to Improve Cell Delivery and Viability. *Stem Cells International* **2016**, 16, <https://doi.org/10.1155/2016/9240652> (2016).
- Kircher, M. F., Gambhir, S. S. & Grimm, J. Noninvasive cell-tracking methods. *Nat Rev Clin Oncol* **8**, 677–688, http://www.nature.com/nrclinonc/journal/v8/n11/supplinfo/nrclinonc.2011.141_S1.html (2011).
- Janic, B. & Arbab, A. S. Cord blood endothelial progenitor cells as therapeutic and imaging probes. *Imaging in medicine* **4**, 477–490, <https://doi.org/10.2217/iim.12.35> (2012).
- Higuchi, T. *et al.* Reporter gene PET for monitoring survival of transplanted endothelial progenitor cells in the rat heart after pretreatment with VEGF and atorvastatin. *J Nucl Med* **50**, 1881–1886, <https://doi.org/10.2967/jnumed.109.067801> (2009).
- Varma, N. R. S. *et al.* Endothelial Progenitor Cells (EPCs) as Gene Carrier System for Rat Model of Human Glioma. *Plos One* **7**, <https://doi.org/10.1371/journal.pone.0030310> (2012).
- Schlechta, B. *et al.* Ex-Vivo Expanded Umbilical Cord Blood Stem Cells Retain Capacity for Myocardial Regeneration. *Circ J* **74**, 188–194, <https://doi.org/10.1253/circj.CJ-09-0409> (2010).

21. Shi, H. *et al.* Tracking of CFSE-labeled endothelial progenitor cells in laser-injured mouse retina. *Chinese Med J-Peking* **124**, 751–757, <https://doi.org/10.3760/cma.j.issn.0366-6999.2011.05.022> (2011).
22. Arbab, A. S. *et al.* Labeling of cells with ferumoxides-protamine sulfate complexes does not inhibit function or differentiation capacity of hematopoietic or mesenchymal stem cells. *NMR in biomedicine* **18**, 553–559, <https://doi.org/10.1002/nbm.991> (2005).
23. Ju, S. *et al.* *In vitro* labeling and MRI of mesenchymal stem cells from human umbilical cord blood. *Magnetic resonance imaging* **24**, 611–617, <https://doi.org/10.1016/j.mri.2005.12.017> (2006).
24. Siow, T. Y., Chen, C. C., Lin, C. Y., Chen, J. Y. & Chang, C. MR phase imaging: sensitive and contrast-enhancing visualization in cellular imaging. *Magnetic resonance imaging* **30**, 247–253, <https://doi.org/10.1016/j.mri.2011.08.008> (2012).
25. Hu, S. L. *et al.* *In vivo* magnetic resonance imaging tracking of SPIO-labeled human umbilical cord mesenchymal stem cells. *Journal of cellular biochemistry* **113**, 1005–1012, <https://doi.org/10.1002/jcb.23432> (2012).
26. Wang, S. *et al.* Magnetic resonance imaging targeting of intracranial glioma xenografts by Resovist-labeled endothelial progenitor cells. *Journal of neuro-oncology* **105**, 67–75, <https://doi.org/10.1007/s11060-011-0569-6> (2011).
27. Willenbrock, S. *et al.* *In vivo* MRI of intraspinally injected SPIO-labelled human CD34+ cells in a transgenic mouse model of ALS. *In vivo (Athens, Greece)* **26**, 31–38 (2012).
28. Mahmoudi, M. *et al.* Novel MRI Contrast Agent from Magnetotactic Bacteria Enables *In Vivo* Tracking of iPSC-derived Cardiomyocytes. *Sci Rep-Uk* **6**, <https://doi.org/10.1038/srep26960> (2016).
29. Diaz, S. & Varki, A. Metabolic radiolabeling of animal cell glycoconjugates. *Curr Protoc Protein Sci* Chapter 12, Unit 12 12 12 11–55, <https://doi.org/10.1002/0471140864.ps1202s57> (2009).
30. Lee, S. Y. *et al.* Non-invasive stem cell tracking in hindlimb ischemia animal model using bio-orthogonal copper-free click chemistry. *Biochem Bioph Res Co* **479**, 779–786, <https://doi.org/10.1016/j.bbrc.2016.09.132> (2016).
31. Hart, C., Chase, L. G., Hajivandi, M. & Agnew, B. Metabolic labeling and click chemistry detection of glycoprotein markers of mesenchymal stem cell differentiation. *Methods Mol Biol* **698**, 459–484, https://doi.org/10.1007/978-1-60761-999-4_33 (2011).
32. Sun, L., Fu, H., Li, Y., Duan, X. & Li, Z. Rapid Recognition and Isolation of Live Colon Cancer Stem Cells by Using Metabolic Labeling of Azido Sugar and Magnetic Beads. *Analytical Chemistry* **88**, 3953–3958, <https://doi.org/10.1021/acs.analchem.6b00154> (2016).
33. Vogt, J. A. *et al.* Protein abundance quantification in embryonic stem cells using incomplete metabolic labelling with ¹⁵N amino acids, matrix-assisted laser desorption/ionisation time-of-flight mass spectrometry and analysis of relative isotopologue abundances of peptides. *Rapid communications in mass spectrometry: RCM* **17**, 1273–1282, <https://doi.org/10.1002/rcm.1045> (2003).
34. Kang, K. *et al.* Tissue-based metabolic labeling of polysialic acids in living primary hippocampal neurons. *Proceedings of the National Academy of Sciences* **112**, E241–E248, <https://doi.org/10.1073/pnas.1419683112> (2015).
35. Lee, S. *et al.* *In vivo* stem cell tracking with imageable nanoparticles that bind bioorthogonal chemical receptors on the stem cell surface. *Biomaterials* **139**, 12–29, <https://doi.org/10.1016/j.biomaterials.2017.05.050> (2017).
36. Agnew, B., Hart, C., Nyberg, T. & Lakshmanaswamy, R. *In vivo* metabolic labeling and detection of specific glycoprotein subclasses in a mouse breast cancer model. *Cancer Research* **67**, 2465–2465 (2007).
37. Laughlin, S. T. & Bertozzi, C. R. Metabolic labeling of glycans with azido sugars and subsequent glycan-profiling and visualization via Staudinger ligation. *Nat. Protocols* **2**, 2930–2944 (2007).
38. Tian, Y. & Zhang, H. Characterization of disease-associated N-linked glycoproteins. *Proteomics* **13**, 504–511, <https://doi.org/10.1002/pmic.201200333> (2013).
39. Dube, D. H., Prescher, J. A., Quang, C. N. & Bertozzi, C. R. Probing mucin-type O-linked glycosylation in living animals. *Proceedings of the National Academy of Sciences of the United States of America* **103**, 4819–4824, <https://doi.org/10.1073/pnas.0506855103> (2006).
40. Kim, E. J. *et al.* Characterization of the Metabolic Flux and Apoptotic Effects of O-Hydroxyl- and N-Acyl-modified N-Acetylmannosamine Analogs in Jurkat Cells. *Journal of Biological Chemistry* **279**, 18342–18352, <https://doi.org/10.1074/jbc.M400205200> (2004).
41. Saki, N., Jalalifar, M. A., Soleimani, M., Hajizamani, S. & Rahim, F. Adverse Effect of High Glucose Concentration on Stem Cell Therapy. *International Journal of Hematology-Oncology and Stem Cell Research* **7**, 34–40 (2013).
42. Follmar, K. E. *et al.* Effects of glutamine, glucose and oxygen concentration on the metabolism and proliferation of rabbit adipose-derived stem cells. *Tissue engineering* **12**, 3525–3533, <https://doi.org/10.1089/ten.2006.12.3525> (2006).
43. Purcell, M. K. *et al.* Identification of the major capsid protein of erythrocytic necrosis virus (ENV) and development of quantitative real-time PCR assays for quantification of ENV DNA. *J Vet Diagn Invest* **28**, 382–391, <https://doi.org/10.1177/1040638716646411> (2016).
44. Rowland, T. J. *et al.* Roles of integrins in human induced pluripotent stem cell growth on Matrigel and vitronectin. *Stem cells and development* **19**, 1231–1240, <https://doi.org/10.1089/scd.2009.0328> (2010).
45. Rodgers, S. J., Ferguson, D. T., Mitchell, C. A. & Ooms, L. M. Regulation of PI3K effector signalling in cancer by the phosphoinositide phosphatases. *Bioscience Rep* **37**, <https://doi.org/10.1042/Bsr20160432> (2017).
46. Soncin, F. & Ward, C. M. The Function of E-Cadherin in Stem Cell Pluripotency and Self-Renewal. *Genes* **2**, 229–259, <https://doi.org/10.3390/genes2010229> (2011).
47. Li, L., Bennett, S. A. L. & Wang, L. Role of E-cadherin and other cell adhesion molecules in survival and differentiation of human pluripotent stem cells. *Cell Adhesion & Migration* **6**, 59–70, <https://doi.org/10.4161/cam.19583> (2012).
48. Bindu, H. & Srilatha, B. Potency of various types of stem cells and their transplantation. *J Stem Cell Res Ther* **1** (2011).
49. Voyta, J. C., Via, D. P., Butterfield, C. E. & Zetter, B. R. Identification and isolation of endothelial cells based on their increased uptake of acetylated-low density lipoprotein. *The Journal of cell biology* **99**, 2034–2040 (1984).
50. Marks, P. W., Witten, C. M. & Califf, R. M. Clarifying Stem-Cell Therapy's Benefits and Risks. *New Engl J Med* **376**, 1007–1009, <https://doi.org/10.1056/NEJMp1613723> (2017).
51. Adamiak, M., Madeja, Z. & Zuba-Surma, E. K. In *Adult Stem Cell Therapies: Alternatives to Plasticity* (ed Mariusz Z. Ratajczak) 35–51 (Springer New York, 2014).
52. Han, S.-S. *et al.* Physiological Effects of Ac4ManNAz and Optimization of Metabolic Labeling for Cell Tracking. *Theranostics* **7**, 1164–1176, <https://doi.org/10.7150/thno.17711> (2017).
53. Roth, Z., Yehezkel, G. & Khalaila, I. Identification and Quantification of Protein Glycosylation. *International Journal of Carbohydrate Chemistry* **2012**, 10, <https://doi.org/10.1155/2012/640923> (2012).
54. Comer, F. I. & Hart, G. W. O-Glycosylation of Nuclear and Cytosolic Proteins: DYNAMIC INTERPLAY BETWEEN O-GlcNAc AND O-PHOSPHATE. *Journal of Biological Chemistry* **275**, 29179–29182, <https://doi.org/10.1074/jbc.R000010200> (2000).
55. Hang, H. C., Yu, C., Kato, D. L. & Bertozzi, C. R. A metabolic labeling approach toward proteomic analysis of mucin-type O-linked glycosylation. *Proceedings of the National Academy of Sciences* **100**, 14846–14851, <https://doi.org/10.1073/pnas.2335201100> (2003).
56. Vocadlo, D. J., Hang, H. C., Kim, E. J., Hanover, J. A. & Bertozzi, C. R. A chemical approach for identifying O-GlcNAc-modified proteins in cells. *Proc Natl Acad Sci USA* **100**, 9116–9121, <https://doi.org/10.1073/pnas.1632821100> (2003).
57. Chang, P. V. *et al.* Metabolic labeling of sialic acids in living animals with alkynyl sugars. *Angew Chem Int Ed Engl* **48**, 4030–4033, <https://doi.org/10.1002/anie.200806319> (2009).
58. Zhao, X. *et al.* Labeling of Enveloped Virus via Metabolic Incorporation of Azido Sugars. *Bioconjug Chem* **26**, 1868–1872, <https://doi.org/10.1021/acs.bioconjchem.5b00310> (2015).
59. Hayakawa, K. *et al.* Epigenetic switching by the metabolism-sensing factors in the generation of orexin neurons from mouse embryonic stem cells. *The Journal of biological chemistry* **288**, 17099–17110, <https://doi.org/10.1074/jbc.M113.455899> (2013).

60. Chen, L. & Liang, J. F. Metabolic Monosaccharides Altered Cell Responses to Anticancer Drugs. *European journal of pharmaceuticals and biopharmaceutics: official journal of Arbeitsgemeinschaft fur Pharmazeutische Verfahrenstechnik e. V* **81**, 339–345, <https://doi.org/10.1016/j.ejpb.2012.03.012> (2012).
61. Baskin, J. M. & Bertozzi, C. R. Bioorthogonal click chemistry: covalent labeling in living systems. *QSAR & Combinatorial Science* **26**, 1211–1219 (2007).
62. van Geel, R., Pruijn, G. J., van Delft, F. L. & Boelens, W. C. Preventing thiol-yne addition improves the specificity of strain-promoted azide-alkyne cycloaddition. *Bioconjugate chemistry* **23**, 392–398, <https://doi.org/10.1021/bc200365k> (2012).
63. Jewett, J. C., Sletten, E. M. & Bertozzi, C. R. Rapid Cu-Free Click Chemistry with Readily Synthesized Biarylazacyclooctynes. *Journal of the American Chemical Society* **132**, 3688–3690, <https://doi.org/10.1021/ja100014q> (2010).
64. Tian, C. *et al.* Use of steric encumbrance to develop conjugated nanoporous polymers for metal-free catalytic hydrogenation. *Chemical Communications* **52**, 11919–11922, <https://doi.org/10.1039/C6CC06372A> (2016).
65. Dommerholt, J. *et al.* Readily accessible bicyclononynes for bioorthogonal labeling and three-dimensional imaging of living cells. *Angewandte Chemie (International ed. in English)* **49**, 9422–9425, <https://doi.org/10.1002/anie.201003761> (2010).
66. Madl, C. M. & Heilshorn, S. C. Bioorthogonal Strategies for Engineering Extracellular Matrices. *Advanced Functional Materials* **28**, 1706046 (2018).
67. Teo, C. F. & Wells, L. Monitoring protein O-linked β -N-acetylglucosamine status via metabolic labeling and copper-free click chemistry. *Analytical biochemistry* **464**, 70–72 (2014).
68. Akiyama, S. K. Integrins in cell adhesion and signaling. *Human cell* **9**, 181–186 (1996).
69. Ellis, S. J. & Tanentzapf, G. Integrin-mediated adhesion and stem-cell-niche interactions. *Cell and Tissue Research* **339**, 121, <https://doi.org/10.1007/s00441-009-0828-4> (2009).
70. Redmer, T. *et al.* E-cadherin is crucial for embryonic stem cell pluripotency and can replace OCT4 during somatic cell reprogramming. *EMBO Reports* **12**, 720–726, <https://doi.org/10.1038/embor.2011.88> (2011).
71. Finney, M. R. *et al.* Direct comparison of umbilical cord blood versus bone marrow-derived endothelial precursor cells in mediating neovascularization in response to vascular ischemia. *Biology of blood and marrow transplantation: journal of the American Society for Blood and Marrow Transplantation* **12**, 585–593, <https://doi.org/10.1016/j.bbmt.2005.12.037> (2006).
72. Lee, M. J. *et al.* Enhancement of wound healing by secretory factors of endothelial precursor cells derived from human embryonic stem cells. *Cytotherapy* **13**, 165–178, <https://doi.org/10.3109/14653249.2010.512632> (2011).

Acknowledgements

This work supported by grants (NRF-2017M3A9C 7065685 and NRF-2016M3A9B4919616) from National Research Foundation funded by the Ministry of Science and ICT, Korea, and the Research Center for High Quality Livestock Products through Agriculture, Ministry of Agriculture, Food and Rural Affairs (Grant no. 715003-07). We thank Eun Hee Han (Korea Basic Science Institute) and Yong-Jin Kim (AMOREFPACIFIC) for technical support in analyses.

Author Contributions

S.-S.H. and H.-E.S. conceived the study and designed most experiments. H.-E.S. and S.-J.P. carried out isolation and *in-vitro* culture of hUCB-EPCs. S.-S.H. and H.-E.S. performed *in-vitro* cell labeling and an analysis of basic cellular properties. S.-S.H. and B.-C.K. analyzed the gene expression patterns of metabolic labeled hUCB-EPCs. D.-E.L. carried out the cell permeability analysis. S.-J.P., H.-M.C. and S.-W.M. analyzed the flow cytometry analysis. All authors analyzed the data and contributed the manuscript preparation. S.-S.H., S.-H.M. and S.-W.K. wrote the manuscript, which was reviewed and edited by the other co-authors.

Additional Information

Supplementary information accompanies this paper at <https://doi.org/10.1038/s41598-018-31594-0>.

Competing Interests: The authors declare no competing interests.

Publisher's note: Springer Nature remains neutral with regard to jurisdictional claims in published maps and institutional affiliations.



Open Access This article is licensed under a Creative Commons Attribution 4.0 International License, which permits use, sharing, adaptation, distribution and reproduction in any medium or format, as long as you give appropriate credit to the original author(s) and the source, provide a link to the Creative Commons license, and indicate if changes were made. The images or other third party material in this article are included in the article's Creative Commons license, unless indicated otherwise in a credit line to the material. If material is not included in the article's Creative Commons license and your intended use is not permitted by statutory regulation or exceeds the permitted use, you will need to obtain permission directly from the copyright holder. To view a copy of this license, visit <http://creativecommons.org/licenses/by/4.0/>.

© The Author(s) 2018